7
Passive and Active Micromixers*

Zhigang Wu and Nam-Trung Nguyen

7.1
Introduction

Micromixers can generally be categorized as passive micromixers and active micromixers [1] (Figure 7.1). The mixing process in passive micromixers relies entirely on molecular diffusion or on chaotic advection of the flow in the mixing channel or chamber. Apart from the forces required for driving the flow, no further external energy is required for mixing. According to the arrangement of the mixed phases, passive mixers can be further categorized into several types: lamination, chaotic advection and droplet. Lamination micromixers can be further divided into serial and parallel types. The injection micromixer is considered as a parallel lamination micromixer. In contrast to passive micromixers, the mixing process in active micromixers relies on disturbances generated by an external field. Active mixers can be categorized based on the source of disturbances: pressure, electrohydrodynamics (including dielectrophoretics and electrokinetics), magnetohydrodynamics, acoustics and thermal field disturbance. Due to the induced external fields and the corresponding integrated active components, the structures of active micromixers are often complicated and require complex fabrication processes. Furthermore, active micromixers require external power sources for their operation. Therefore, it is both challenging and expensive to integrate active micromixers into a microfluidic system. In contrast, passive micromixers have simpler structures and do not require external actuators except those for fluid delivery as in active micromixers. The often simple passive structures are robust, stable in operation and easy to integrate into a system. For the above-mentioned reasons, more attention is given to passive micromixers.

Previously, the fabrication of micromixers was based on microsystem technology or microelectromechanical system (MEMS) technology, which focused on hard materials such as silicon and glass [2]. Recently, polymers have been extensively used for fabricating micromixers. Polymers have several advantages over silicon and

*A List of Symbols and Abbreviations can be found at the end of this chapter.

Micro Process Engineering, Vol.1: Fundamentals, Operations and Catalysts
Edited by V. Hessel, A. Renken, J.C. Schouten, and J.-I. Yoshida

ISBN: 978-3-527-31550-5

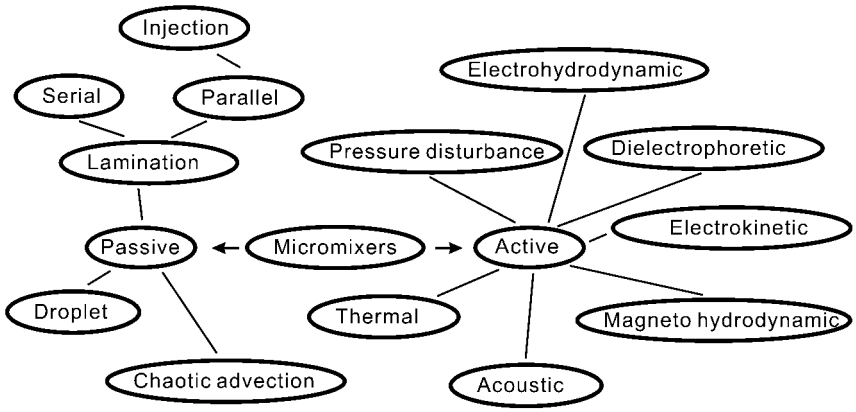

Figure 7.1 Classification of micromixers.

glass, such as low cost of both materials and fabrication, degradability and biocompatibility. A number of polymeric fabrication techniques such as hot embossing, injection molding, casting, laser ablation and surface micromachining are readily available for large-scale industrial and academic research.

Micromixers can either be integrated in a microfluidic system or work as standalone devices. Furthermore, investigation of micromixers is fundamental for understanding transport phenomena on the microscale. This chapter provides information on the latest advances in micromixing technology. Readers can also refer to some earlier review articles and book chapters, such as [1, 3–7]. For general references on mixing, there are some excellent books and review papers available. The theory on thermal motion of molecules proposed by Einstein is the foundation for diffusion theory [8]. For macroscale mixing [9], the two common mixing methods are the generation of turbulence [10] and chaotic advection [11, 12]. Introducing turbulence in a mixer makes fluid motions vary irregularly. This random movement causes the components inside the device to mix together quickly. Chaotic advection can be generated by splitting, stretching, folding and breaking up a laminar flow, which is very effective at small Reynolds numbers. For more elaborate and focused work on diffusion theory and various transport phenomena, the reader can refer to [13–15], which are useful for understanding the fundamentals of species transport and flow behavior in micromixers.

Since different types of micromixers have different operating conditions, this chapter considers and discusses various micromixer types separately. Depending on the particular mixer types, attention is paid to a number of operating parameters such as Reynolds number (*Re*) and Peclet number (*Pe*). The Reynolds number:

$$Re = \frac{U D_{\mathrm{h}}}{\nu} \tag{7.1}$$

represents the ratio between the momentum and the viscous friction, where U is the average velocity of the fluid, D_{h} is the hydrodynamic diameter and ν is the kinetic viscosity of the fluid. A high Reynolds number above a critical value (2300 on the

macroscale) indicates a turbulent flow. Due to small Reynolds numbers, laminar flow can be expected in most micromixers. The Peclet number:

$$Pe = \frac{UL}{D} \tag{7.2}$$

represents the ratio between convective and diffusive species transport, where L is the mixing path and D is the diffusion coefficient between the species. A large Peclet number indicates that convection is more dominant.

7.2 Passive Micromixers

Owing to its simple concept and low requirements for fabrication processes, the passive mixer was one of few first reported microfluidic devices. Because of the laminar flow on the microscale, mixing in passive micromixers relies mainly on two mechanisms: molecular diffusion and chaotic advection. Molecular diffusion is always the final mixing stage in all micromixers. Increasing the contact surface between the mixing fluids and decreasing the diffusion path between them lead to enhancement of diffusive transport. Chaotic advection can be realized by methods that exist on the macroscale for highly viscous fluids.

7.2.1 Parallel Lamination Micromixers

As mentioned above, mixing can be enhanced by decreasing the mixing path and increasing the contact surface between the two flows. Parallel lamination splits the inlet streams into substreams of n. In the basic case, n is equal to 2. Parallel lamination mixers with two streams are also called T-mixers or Y-mixers [16–18] (Figure 7.2a and b). When the mixing channel width W is far larger than its height H, an analytical solution for the concentration distribution in the mixing channel can be derived (Figure 7.3a). Assuming the same viscosity and a resulting uniform flow velocity U inside the mixing channel, the dimensionless concentration distribution $c^* = c/C_0$ between a solute ($c = C_0$) and a solvent ($c = 0$) with an arbitrary mixing ratio r is

$$c^*(x^*, y^*) = r + \frac{2}{\pi}\sum_{n=1}^{\infty}\frac{\sin n r\pi}{n}\cos(n\pi y^*)\exp\left(-\frac{2n^2\pi^2}{Pe + \sqrt{Pe^2 + 4n^2\pi^2}}x^*\right)$$
$$n = 1, 2, 3, \ldots \tag{7.3}$$

where $x^* = x/W$, $y^* = y/W$ are dimensionless coordinates (Figure 7.3a). The solution in Equation (7.3) [19] (Figure 7.3b) can be extended for the case of parallel lamination with multiple streams [20] (Figure 7.3c). The inlet streams of a T-mixer can be twisted and laminated as two thin liquid sheets to reduce the mixing path [21]. Because of its simple configuration, the T-mixer is ideal for investigations of basic transport

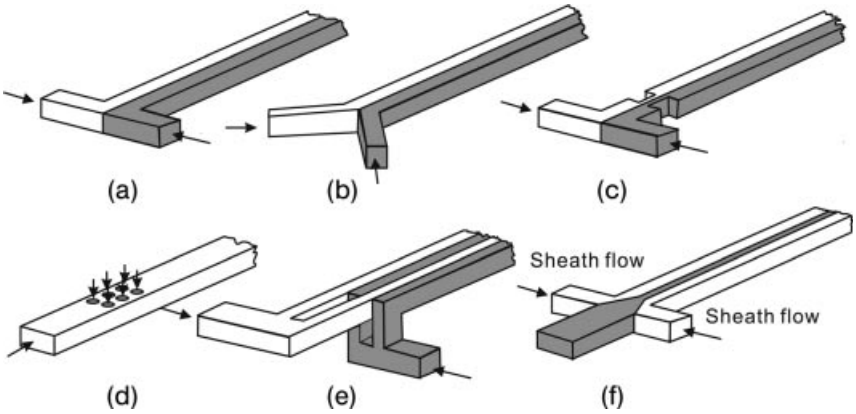

Figure 7.2 Parallel lamination micromixers: (a) basic T-mixer; (b) Y-mixer; (c) mixer with a throat; (d) concept of injection mixer; (e) concept of parallel lamination; (f) and concept of hydraulic focusing.

phenomena in microfluidics such as the butterfly effect [16], scaling law [18] and other non-linear effects [19].

Since molecular diffusion is a slow process even on the microscale, generally a T-mixer has a long mixing channel and a corresponding long mixing time. Apart from the introduction of lamination of multiple streams, good mixing could also be

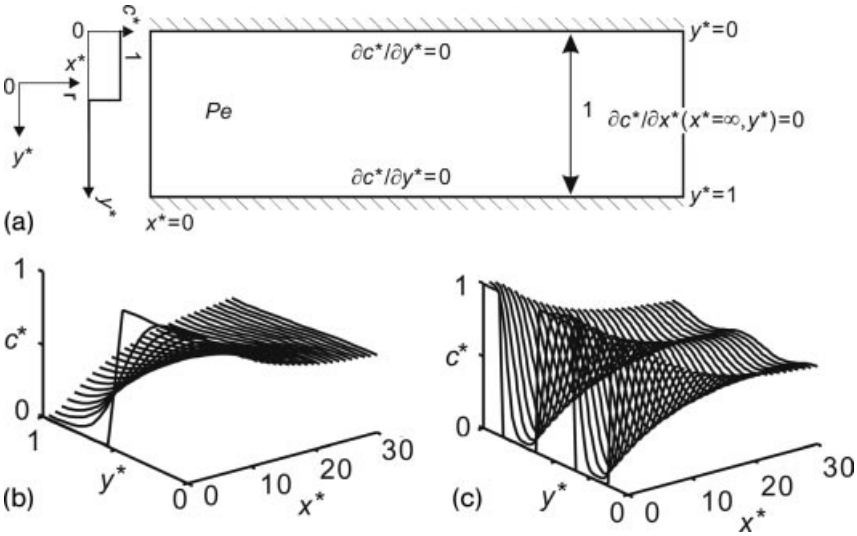

Figure 7.3 Concentration distribution in **a** parallel lamination micromixer: (a) the dimensionless 2D model; (b) result for Y-mixer ($n = 1$, $r = 0.5$); (c) result for parallel animation mixer with multiple streams ($n = 5$, $r = 0.5$).

achieved with a short mixing length at an extremely high Reynolds number [22, 23]. The resulting chaotic advection or vortices are expected to enhance mixing efficiently at these high *Re*. In [22], vortices were generated at *Re* above 10. When *Re* was higher than 30, good mixing was achieved right after the bend of the mixing channel. Adopting a planar spiral channel [24], the Dean flow effect was used to achieve good mixing at *Re* above 10. Wong *et al.* [23] utilized *Re* up to 500 in a T-mixer with flow velocity as high as 7.60 ms^{-1} and driven pressure up to 7 bar. In a diamond-shaped cavity close to a straight microchannel, a fluid flow can also generate high shear to drive very fast circulation under extremely high *Re* ($Re = 245$, 45 ms^{-1}) [25]. Fast vortices can be obtained with multiple inlet streams focused in a circular chamber for fast mixing [26, 27]. In these micromixers, the velocities were on the order of 1 ms^{-1} (7.6 ms^{-1} in [23]), 10 ms [26] or even higher (up to 45 ms^{-1} in [25]) and required high driving pressures. These high pressures (1.0–5.5 bar in [23], 15 bar in [26]) challenged the present bonding and interconnection technologies. Roughening the channel wall [28] or throttling the channel entrance [29] (Figure 7.2c) could also benefit the mixing in a T-mixer. In addition, 3D vortices can be generated in a surface tension-driven mixing chamber [30]. However, the operating parameters such as velocity and *Re* were not reported.

A simple approach to reducing the mixing path is to make a narrow mixing channel [31, 32], which can be realized by adopting parallel lamination with multiple streams [33–35] (Figure 7.2e) or with 3D interdigitated mixing streams [36]. A parallel lamination mixer with 32 streams can achieve full mixing in 15 ms [37]. This mixer type was successfully used in a practical analysis [38]. The flows in micromixers based on parallel lamination are usually driven by pressure, but can also be driven by electroosmosis [39–41]. The concept of an injection mixer (Figure 7.2d) [42–45] is a special parallel lamination mixer. This mixer type only splits one of the inlet flows into many streams and injects them into the other flow stream. An array of nozzles was used to create a number of microplumes. These plumes decrease the mixing path and increase the contact surface between the two inlet flows to the same extent. In [42], 400 nozzles were designed in a square array in a mixing chamber fabricated in silicon using deep reactive ion etching (DRIE). Larsen *et al.* [43] demonstrated a different nozzle shape with a similar concept. In [44] and [45], microplumes were achieved by using capillary forces.

Another concept for reducing the mixing path for parallel lamination micromixers is hydrodynamic focusing [46]. The basic design for hydrodynamic focusing is a long microchannel with three inlets. The middle inlet is for the sample flow, while the solvent streams join through the other two inlets and work as the sheath flows (Figure 7.2f). Assuming that two fluids with η_1 and η_2 are sandwiched in a channel with width $2W$ and height H, the velocity distribution u_1 and u_2 in the channel can be described by the Navier–Stokes equations [47]:

$$\begin{aligned} \frac{\partial^2 u_1}{\partial y^2} + \frac{\partial^2 u_1}{\partial z^2} &= \frac{1}{\eta_1}\frac{\partial p}{\partial x} \\ \frac{\partial^2 u_2}{\partial y^2} + \frac{\partial^2 u_2}{\partial z^2} &= \frac{1}{\eta_2}\frac{\partial p}{\partial x} \end{aligned} \tag{7.4}$$

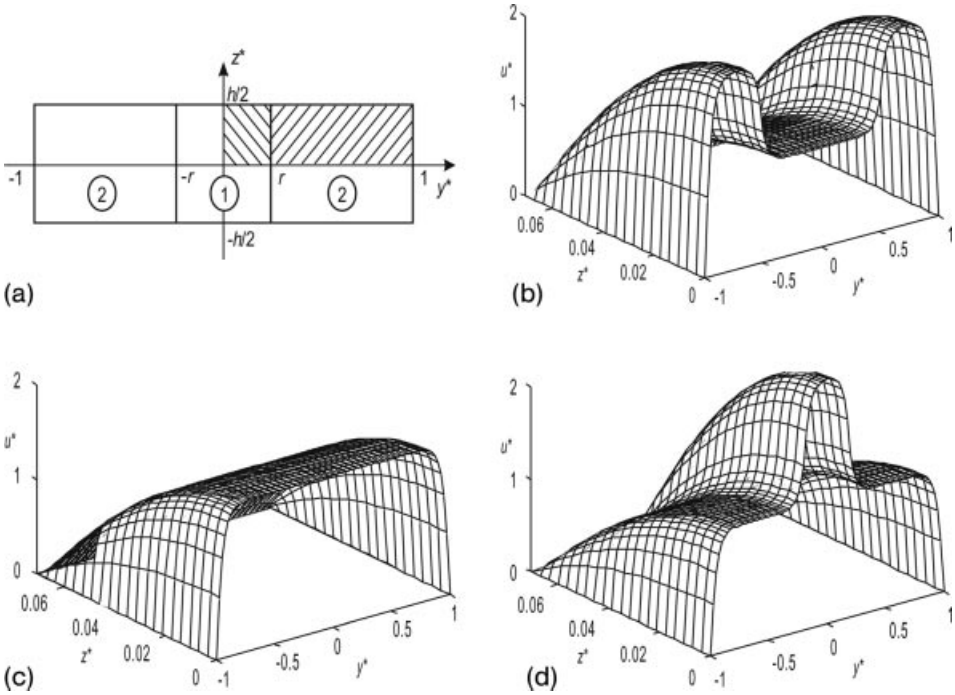

Figure 7.4 Hydrodynamic focusing: (a) the dimensionless 2D model and (b–d) the dimensionless velocity profile ($h = 0.14$, $\kappa = 1$); (b) $\beta = 0.5$; (c) $\beta = 1$; (d) $\beta = 2$.

where r is the dimensionless position of the interface and subscripts 1 and 2 represent the sample flow and the sheath flow, respectively. Owing to natural symmetries, one-quarter of the cross-section needs to be considered. Normalizing the velocity by a reference velocity u_0 and the coordinates by W leads to the following dimensionless model (Figure 7.4a):

$$\begin{aligned} \frac{\partial^2 u_1^*}{\partial y^{*2}} + \frac{\partial^2 u_1^*}{\partial z^{*2}} &= \frac{W}{\eta_1 u_0}\frac{\partial p}{\partial x^*} \\ \frac{\partial^2 u_2^*}{\partial y^{*2}} + \frac{\partial^2 u_2^*}{\partial z^{*2}} &= \frac{W}{\eta_2 u_0}\frac{\partial p}{\partial x^*} \end{aligned} \tag{7.5}$$

With $P' = \frac{W}{\eta_1 u_0}\frac{\partial p}{\partial x^*}\beta = \eta_2/\eta_1\ \theta = (2n-1)\pi/h$, the solutions of Equation (7.5) have the following forms ($0 < y^* < 1,\ 0 < z^* < h/2$):

$$\begin{aligned} u_1^*(y^*, z^*) &= P'\left[\frac{z^{*2} - h^2/4}{2} + \sum_{n=1}^{\infty} \cos\theta z^* (A_1 \cosh \theta y^* + B_1 \sinh \theta y^*)\right] \\ u_2^*(y^*, z^*) &= \frac{P'}{\beta}\left[\frac{z^{*2} - h^2/4}{2} + \sum_{n=1}^{\infty} \cos\theta z^* (A_2 \cosh \theta y^* + B_2 \sinh \theta y^*)\right] \end{aligned} \tag{7.6}$$

For a flat channel ($h \ll 1$), the position of the interface can be estimated as

$$r = \frac{1}{1 + 2\beta\kappa} \tag{7.7}$$

where $\kappa = Q_2/Q_1$ is the flow rate ratio between the one sheath stream and the sample stream. A Fourier analysis with the above boundary conditions results in the coefficients of Equation (7.6):

$$\begin{aligned} A_1 = D[&\beta \sinh\theta r \cosh^2\theta r \cosh\theta - \sinh^3\theta r \cosh\theta \\ &-(\beta-1)\sinh^2\theta r \sinh\theta \cosh\theta - (\beta-1)\sinh^2\theta r(\cosh\theta - \cosh\theta r) \\ &+(\beta-1)\sinh\theta r \cosh\theta r \cosh\theta(\cosh\theta - \cosh\theta r)]/ \\ &[\beta \cosh^2\theta r \sinh\theta r \cosh^2\theta - \sinh^3\theta r \cosh^2\theta - \\ &(\beta-1)\sinh^2\theta r \cosh\theta r \sinh\theta \cosh\theta] \end{aligned} \tag{7.8}$$

$$\begin{aligned} A_2 = D[&\beta \cosh^2\theta r \cosh\theta - \sinh^2\theta r \cosh\theta - (\beta-1)\sinh\theta r \cosh\theta\, r \sinh\theta \\ &-(\beta-1)\sinh\theta r \cosh\theta r \cosh\theta(\cosh\theta - \cosh\theta r)]/ \\ &[\beta \cosh^2\theta r \sinh^2\theta - \sinh^2\theta r \cosh^2\theta - \\ &(\beta-1)\sinh\theta r \cosh\theta r \sinh\theta \cosh\theta] \end{aligned} \tag{7.9}$$

$$B_1 = 0 \tag{7.10}$$

$$\begin{aligned} B_2 = D[&(\beta-1)\sinh\theta r(\cosh\theta - \cosh\theta r)]/ \\ &[\beta \cosh^2\theta r \cosh\theta - \sinh^2\theta r \cosh\theta - \\ &(\beta-1)\sinh\theta r \cosh\theta r \sinh\theta] \end{aligned} \tag{7.11}$$

where

$$D = (-1)^{n+1} \frac{4h^2}{(2n-1)^3\pi^3}$$

The velocity of the sample flow is lower, if the sample flow is more viscous than the sheath flow ($\beta < 1$) (Figure 7.4b). If the viscosities are equal ($\beta = 1$), the flows behaves as a single phase, (Figure 7.4c). If the sheath flows are more viscous ($\beta > 1$), the sample flow is faster, (Figure 7.4d). From the above results, the sample fluid can be focused to a narrow width by adjusting the flow rate or/and viscosity ratio between the sample flow and the sheath flow. Hydrodynamic focusing reduces the stream width, and consequently the mixing path.

In [46], the prototype has a mixing channel of $10 \times 10\,\mu m$ cross-section. The focusing width was adjusted by the pressure ratio applied on the sheath and sample flow. The mixing time can be reduced to a few microseconds [48]. Hydrodynamic focusing and mixing were used for cell infection as reported in [49]. In [50], focusing using an immiscible fluid was utilized to obtain rapid mixing. Multiple reagent mixing could be achieved using focusing structure [51]. Focusing structure could be used in droplet mixing, which will be discussed later. Tables 7.1 and 7.2 list the typical parameters for parallel and injection micromixers, respectively.

Table 7.1 Typical parallel lamination micromixers.

Ref.	Type	Channel width (μm)	Channel height (μm)	Typical velocity (mm s^{-1})	*Re*	*Pe*	Material
Kamholz [16, 17]	T-mixer	550	25	6	0.3	725	Silicon–glass
Ismagilov [18]	Y-mixer	90	90	7	0.4	240	PDMS–glass
Wu [19]	Y-mixer	900	50	0.27	0.02	150	PMMA–acrylics
Hinsmann [21]	Y-mixer	1000	20	83	1.7	830	CaF_2–SU8–metal–glass
Yi [22]	Y-mixer	200	200	50–200	80	80 000	Ceramic
Wong [23]	T-mixer	100	50	7000	500	700 000	Silicon–glass
Sudarsan [24]	Y-mixer (Dean flow)	150	29	4–372	0.02–18.6	20–18 600	SEBS–SEBS
Böhm [26]	Vortex	20	200	10000	200	200 000	Silicon–glass
Lin [27]	Vortex	830	1000	8.7–300	0.5–17.1	500–17 100	Glass
Wong [28]	Cross-shaped	30	40	5000–10 000	170–340	150 000	Ceramic
Gobby [29]	T-mixer	500	300	0.3	0.1	150	NA[a]
Veenstra [31]	T-mixer	100	200	0.17	0.023	170	Silicon–glass
Lee [32]	T-mixer	300	10	667	13.3	13 300	PDMS
Koch [35]	Parallel lamination	85	5	0.7	0.0035	60	Silicon–glass
Bessoth [37]	Parallel lamination	20	50	1.5	0.07	60	Glass
Hadd [40]	T-mixer	35	9	1	0.014	35	Glass
Knight [46]	Focusing	10	10	50	0.5	500	Silicon–PDMS–glass
Wu [47, 50]	Focusing	900	50	1	0.05	100	PMMA–acrylics
Walker [49]	Focusing	200–1000	150	1	0.15	200	PDMS–glass
Park [51]	Focusing	50	100	1–1000	0.067–66.7	67–66 700	Zeonor COC

[a]NA, not applicable; SEBS, polystyrene–(polyethylene/polybutylene)–polystyrene triblock copolymer.

Table 7.2 Typical injection micromixers.

Ref.	No. of nozzles	Channel width (μm)	Nozzle size (μm)	Channel height (μm)	Typical velocity (mms^{-1})	*Re*	*Pe*	Materials
Miyake [42]	400	2000	330	15×15	1.2	0.018	18	Silicon–glass
Larsen [43]	10–20	NR[a]	ϕ100	50	1	0.1	100	Silicon–glass
Seidel [44]	1	280–600	135–175	20–43	NR	NR	NR	Silicon–glass
Voldman [45]	1	820	7	70	15	0.1	105	Silicon–glass

[a]NR, not reported.

7.2.2 Serial Lamination Micromixers

Mixing can also be enhanced by serial lamination via splitting and later joining the substreams (Figure 7.5a) [52–55]. The inlet streams are first joined horizontally and then twisted vertically in the next stage. Through splitting and joining m stages, 2^m laminated liquid layers can be achieved. The process leads to a 4^{m-1} times improvement in mixing time. The mixers in [52–54] (Figure 7.5b) were fabricated via wet etching in KOH or the DRIE technique in silicon. The same approach can be realized using polymer materials [55] (Figure 7.5c). As serial lamination micromixer can also be achieved using electrokinetic flows [56] (Figure 7.5d). Introducing electroosmosis flows between the multiple intersecting microchannels, the mixing was enhanced significantly. In [57], a similar design was demonstrated under a pressure-driven flow. However, this approach is only suitable for a plug of the two mixing liquids. Table 7.3 compares the typical parameters for serial parallel micromixers.

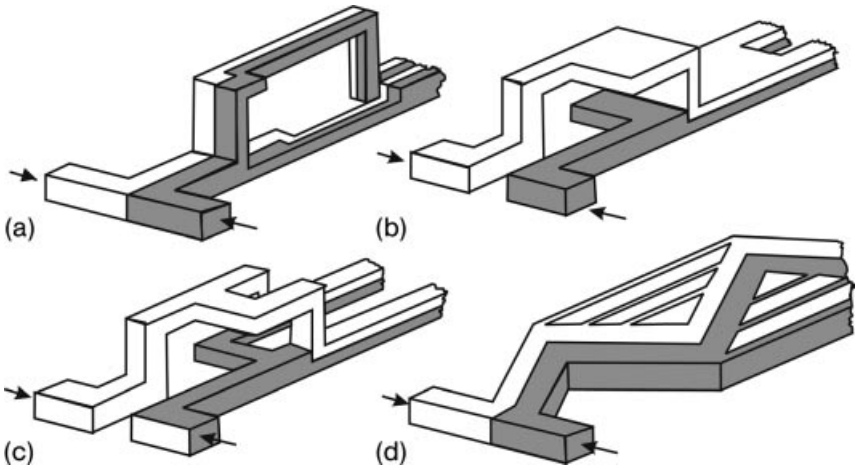

Figure 7.5 Serial lamination mixer: (a) join–split–join; (b) split–join [52]; (c) split–split–join [55]; (d) multiple intersecting microchannels [56] .

Table 7.3 Typical serial lamination micromixers.

Ref.	Number of stages	Channel width (μm)	Channel height (μm)	Typical velocity (mm/s)	*Re*	*Pe*	Materials
Branebjerg [52]	3	300	30	1–22	0.03–0.66	15–330	Silicon–glass
Schwesinger [53]	5–20	400	400	1.8	0.072	72	Silicon–glass
Gray [54]	6	200	100	NR[a]	NR	NR	Silicon–glass
Munson [55]	6	600	100	0.5	0.05	50	Mylar
He [56]	1	100	10	0.25	0.0025	25	Quartz
Melin [57]	16	50	50	2	0.1	14	Silicon–PDMS

[a]NR, not reported.

7.2.3 Micromixers Based on Chaotic Advection

In general, advection is often parallel to the main flow direction, and mixing processes prefer transversal transport. By introducing transversal flow between the mixing species, the so-called chaotic advection can be used to improve the mixing process. Since the advection is far stronger than diffusion even on the microscale, chaotic advection is widely used in designing micromixers. Naturally, chaotic advection can be induced by an external force and will be discussed later under active mixers. On the macroscale, chaotic advection can also be generated by specific geometries in the mixing channel or chambers. The basic idea is splitting, stretching, folding and breaking of the flow via the modification of the channel shape, which are well investigated and summarized in [12]. However, this mechanism was ignored for a long time in the earlier development of micromixers because people took laminar flow for granted in microfluidics. With relative structure and versatile working conditions (working from very low *Re* such as a few one thousandths to high *Re* such as a few hundred), the development of passive micromixers based on chaotic advection attracted a lot of attention and progressed rapidly in recent years. In the following, micromixers working at different ranges of *Re* are discussed. The ranges $Re > 100$ is considered high, $10 < Re < 100$ intermediate and $Re < 10$ low [1].

7.2.3.1 Chaotic Advection at High Reynolds Numbers

The simplest method to generate chaotic advection is to introduce obstacle structures in the mixing channel. A numerical investigation of obstacles at high *Re* was reported in [58]. The simulated diameter of the obstacle was 60 μm within the mixing channel of 300 μm in width, 100 μm in depth and 1.2–2 mm in length (Figure 7.6b). After investigation of many arrangements of obstacles at $Pe = 200$, it was found that eddies or recirculations cannot be generated by introducing obstacles in a microchannel at low *Re*. However, these obstacles could improve the mixing performance at high *Re*. The asymmetric arrangement of obstacles could alter the flow directions and force fluids to merge and create transversal mass transport. In [59], seven cylinders of 10 μm diameter were used to enhance mixing in a $50 \times 100 \times 100$ μm mixing

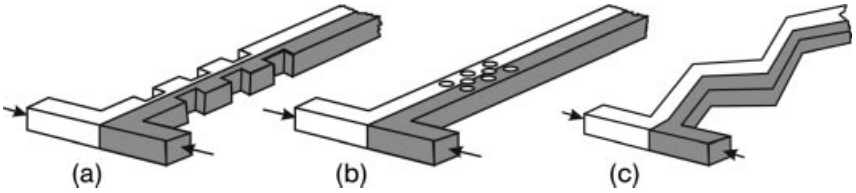

Figure 7.6 Designs examples for mixing with chaotic advection at high Reynolds numbers: (a) obstacles in side wall [28]; (b) obstacles in the channel [59, 77]; (c) zig-zag shaped channel [60].

channel. The micromixer, worked under *Re* from 200 to 2000 and a mixing time of 50 μs. Another approach for generating chaotic advection is to bend the straight mixing channel into a zigzag shape and then produce recirculation around the turns at high *Re*. Based on a numerical investigation, Mengeaud *et al.* [60] discussed the periodic steps of the zigzag shape as the optimisation parameter (Figure 7.6c). The micromixers were fabricated on a poly (ethylene terephthalate) (PET) substrate through excimer laser ablation. The mixing channel had a width of 100 μm, a depth of 48 μm and a length of 2 mm. In the simulation, the *Pe* was fixed at 2600 and *Re* ranged from 0.26 to 267. A critical *Re* of 80 were observed. Above this number, mixing benefited from the generated recirculations at the turns. Below this number, the mixing process relied entirely on molecular diffusion.

In addition, very tiny obstacles inside the mixing chamber similar to the above-mentioned design also could work at very low *Re* ($Re < 1$). In [61], 3D nanosized obstacles posts were formed in an SU-8 structure on a glass substrate. The prototype was covered and fluidic confected by a PDMS layer using cold welding. The post had a 570 nm diameter with 420 nm height and was spaced at 710 nm.

7.2.3.2 **Chaotic Advection at Intermediate Reynolds Numbers**

On the macroscale, chaotic advection could be generated by introducing three-dimensionally twisted conducts [62]. However, in-plane structures, such as modified Tesla [63] and inverse ϕ-shaped oscillator [64], fabricated on the microscale, can produce chaotic advection in for better mixing. In [63], the Coanda effect caused chaotic advection. The mixer was made on the cyclic olefin copolymer (COC) surface via hot embossing and thermal diffusion bonding. In [64], five microfluidic ϕ-shaped oscillators [65] were connected serially to produce chaotic advection and further enhance the mixing process in the chamber. The mixer was fabricated using PDMS elastomer. Although this design can work over a large range of *Re*, it has best performance when *Re* is equal to 14.

In 2000, Liu [66] demonstrated a three-dimensional C-shaped serpentine micromixer made in silicon and glass (Figure 7.7a). This design was adapted from a basic T-mixer with six serially contacted mixing units. The total mixing channel length including the straight channel was about 20 mm. In this design, chaotic advection only occurred at relatively high *Re* ($Re = 25–70$). Vijayendran *et al.* [67] demonstrated a three-dimensional serpentine micromixer made of PDMS. Here, the mixing unit was changed to L-shape, (Figure 7.7b). The mixing channel has a width of 1 mm, a

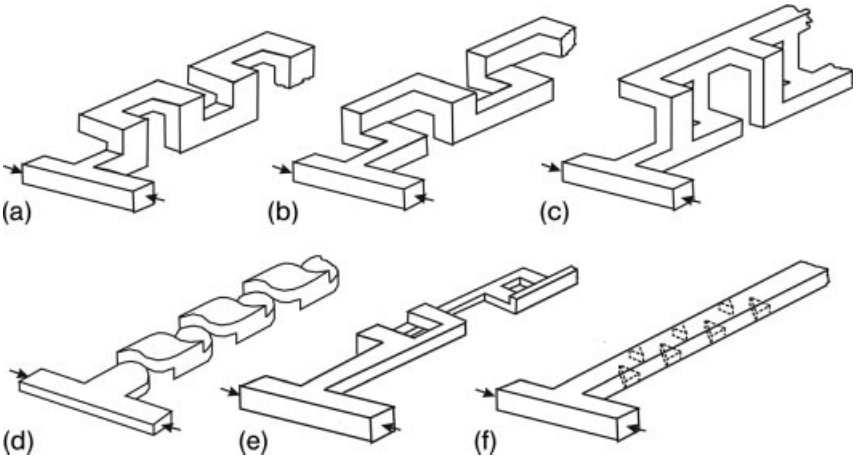

Figure 7.7 Three-dimensional designs with chaotic advection at intermediate *Re*: (a) C-shape [66]; (b) L-shape [67]; (c) connected out-of-plane L-shapes [70]; (d) twisted microchannel [71]; (e) F-shape [68]; (f) alligator's teeth shape [69].

depth of 300 μm and a total mixing length of about 30 mm. The mixing performance was tested at *Re* of 1, 5 and 20. Similarly to the C-and L-shaped designs, the experimental results also indicated that better mixing was achieved at higher *Re*. Later, an F-shaped mixing unit was also proposed [68] (Figure 7.7e). The mixer was fabricated from COC and had a width of 250 μm, a depth of 60 μm and a length of 10 mm. In [69], so-called alligator's teeth were assembled in the mixing channel (Figure 7.7f), but actually it is more like a modified C-shaped channel. This designs had a good performance at lower *Re* ($Re = 8$). In another design on PDMS, the mixing unit, a so-called "flow-folding topological structure", was formed by two connected out-of-plane L-shapes [70] (Figure 7.7c). The mixing channel had a width of 100 μm and a depth of 70 μm. A single mixing unit had a size of 400 × 300 μm. Within this design, effective mixing can be achieved on short length scales at lower *Re* ($Re = 0.1$–2).

A complex three-dimensional micromixer was reported in [71]. This work fully borrowed from the theory on the macroscale [12] to improve mixing on the microscale with complex and fine three-dimensional channel shapes. The mixing channel rotated and separated the two fluids by partitioned walls and generated smaller blobs exponentially (Figure 7.7d). This structure was fabricated with PDMS on glass. In [72], many kinds of twisted channel were investigated numerically withholding fabricated prototypes. The channel had a width of 500 μm and a height of 300 μm. The mixing between methanol and oxygen at different velocities (0.5–2.5 ms^{-1}) was considered in the simulation.

7.2.3.3 Chaotic Advection at Low Reynolds Numbers

Similarly to those in macroscale mixers, rips (Figure 7.8a) or grooves (Figure 7.8b and c) on the channel wall can produce chaotic advection. In [73], the slanted grooves were

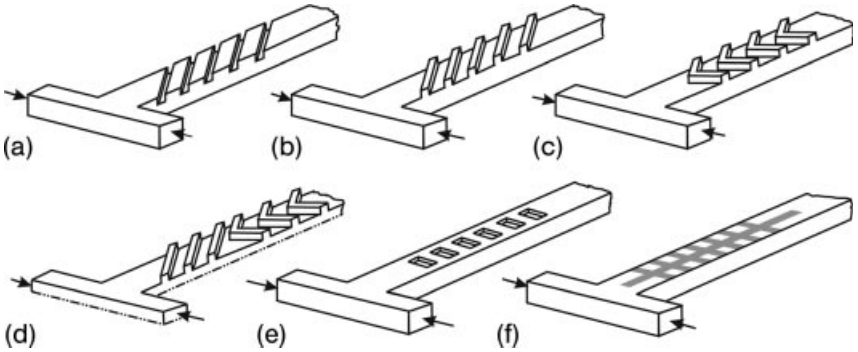

Figure 7.8 Modification of mixing channel for chaotic advection at low *Pe*: (a) slanted ribs, (b) slanted grooves [74, 75], (c) staggered-herringbone grooves [74, 75], (d) patterns on both top and bottom of the mixing channel, (e) groove pattern vertical to mail flow, and (f) one of patterns for surface modification in a micromixer with electrokinetic flows [80].

ablated on the bottom wall on a polycarbonate (PC) sheet via excimer laser ablation and finally covered by a layer of poly (ethylene terephthalate glycol) (PETG). This structure twisted electrokinetic flow into a helix mass stream at a relatively slow velocity of 300 μms^{-1}. The mixing channel was 72 μm wide at the top, 28 μm wide at the bottom and 31 μm deep. The width of groove was 14 μm and the center-to-center spacing between the grooves was 35 μm. The length of the region occupied by the wells from the T-junction was 178 μm.

This configuration can also be extended to pressure-driven micromixers [74]. Two different groove patterns were proposed (Figure 7.8b and c). The so-called staggered herringbone mixer (Figure 7.8b) can work well at *Re* ranging from 1 to 100. Later, this concept was extended to electrokinetic flow by modifying the surface charge [75]. The combination of these two kinds of groove patterns on both the top and bottom wall surfaces was investigated in [76], (Figure 7.8d). The effect of chaotic advection with the ripped channel was numerically investigated by Wang *et al.* [77]. The length, width and depth of the channels were 5 mm, 200 μm, and 100 μm, respectively. The mean velocity ranged from 100 μms^{-1} to 50 mms. The grooves were also ablated on the PDMS substrate by a laser [78]. Further, this slanted groove can be vertical to the main channel direction (Figure 7.8e) and in the form of a 3D shape on the PDMS side wall of the channel by using an inclined multilithography-fabricated SU-8 master [79]. Electrokinetic mixing [80] with only patterned surface modification can also enhance mixing (Figure 7.8f). With a field strength of 70–555 $V cm^{-1}$ along the 1.8 mm long microchannel, mixing efficiencies can be improved by 22–68% at *Pe* 190–1500. The concept of surface modification can be found in [81]. Kim *et al.* [82] found that it was also effective using embedded barriers parallel to the flow direction for the design in [74]. These embedded barriers bring a hyperbolic mixing pattern instead of the original elliptical one in [74]. The mixing channel of this design was 240 μm in width, 60 μm in depth and 21 mm in length. The barriers had a cross-section of 40 × 30 μm.

Borrowing from a conventional mixer with helical elements, a miniaturized version was reported in [83]. This so-called Kenics static mixer [84] utilized the three-dimensional inner surface to introduce chaotic advection in a cylindrical mixing channel. Two designs were demonstrated: the first design was formed by four mixing elements, made of 24 rectangular bars placed at 45°, and the four mixing elements were arranged at 45° in the channel. The second design consisted of right- and left-handed helical elements containing six small-helix structures. Due to the complicated geometry, the micromixer was fabricated via stereo microphotography, which builds up the complex structure layer by layer. The most important parameters for the above-mentioned chaotic advection micromixers are summarized in Table 7.4.

In addition to various geometries, the instability between the multi-miscible fluids can also be used to generate chaotic advection using focusing structure and abrupt divergent channels at low *Re* [85, 86]. Generally, the miscible fluids behave as laminar flow in focusing structure. However, when the viscosity difference between the two miscible flows is large enough, the flow would become unstable and produce complex patterns, which can be used for mixing. Using two kinds of silicone oil with viscosities of 500 and 0.5 cP, the highly folding pattern was generated inside a silicon–glass fabricated microfluidic device [85]. The channel had a width and height of 100 μm. Various viscous folding patterns can be formed in this approach: oscillatory folding folding modified by strong diffusion, heterogeneous folding and subfolding. This folding induced by diverging channels significantly enhances the mixing between liquids with different viscosities. In [86], viscoelastic effects between a more viscous poly(ethylene oxide) (PEO) in glycerol–water and less viscous PEO in water were investigated in a similar structure fabricated in poly(methyl methacrylate) (PMMA). An obvious recirculated pattern was observed in the contract part of the channel and subsequently good mixing was achieved after the divergent channel at low *Re* ($Re = 0.149$) Typical chaotic advection micromixers are summarized in Table 7.4.

7.2.4 Droplet Micromixers

Tiny formed droplets have two natural merits for enhancing the mixing process: first, the process of forming the droplet itself is a process to reduce the distance and increase the contact surface between the mixing species; second, similarly to the rotation of solid particles inside fluids, it is convenient to make droplets recirculate and sequently enhance the mixing of the species inside the droplet by simply modifying the channel shape. The movement of a droplet causes an internal flow field and makes the mixing inside the droplet rapid. Compared with the continuous mixing process, a droplet micromixer affords an isolated microenvironment, which is very suitable for many chemical syntheses and reactions.

Generally, droplets can be generated and transported individually through pressure [87] or capillary effects such as thermocapillary [88] and electrowetting [89]. Furthermore, droplets can be generated in a small channel with multiple immiscible phases such as oil–water or water–gas using a T-shaped structure [90] and focusing

Table 7.4 Typical chaotic advection micromixers.

Ref.	Type	Channel width (μm)	Channel height (μm)	Typical velocity (mms^{-1})	*Re*	*Pe*	Material
Wang [58]	Cylindrical obstacles	300	100	0.17	0.25	51	NA[a]
Lin [59]	Cylindrical obstacles	10	100	20	0.2	200	Silicon–glass
Mengeaud [60]	Zigzag shaped	100	48	1.3–40	0.26–267	130–4000	Mylar
Hong [63]	2D Tesla	200	90	5	6.2	10 000	COC
Jeon [64]	2D inverse ϕ	300	150	70	14	14 000	PDMS
Liu [66]	3D serpentine	300	150	30–350	6–70	9000–10^4	Silicon–glass
Vijayendran [67]	3D serpentine	1000	300	2–40	1–20	2000–4×10^4	PDMS
Chen [70]	3D serpentine	100	70	1–20	0.1–2	10–200	PDMS
Park [71]	3D serpentine	100	50	n/r	1–50	0.015–0.7	PDMS
Jen [72]	3D serpentine	500	300	2000	48	0.36	NA
Kim [68]	3D serpentine	300	200	20.7	8	16 000	PDMS
Johnson [73]	Patterned wall	72	31	0.6	0.024	15	PC–PETG
Stroock [74, 75]	Patterned wall	200	70	15	0.01	3000	PDMS
Wang [77]	Patterned wall	200	100	0.1–50	0.0013–6.65	20–10^4	PDMS
Biddiss [80]	Patterned wall	200	8	0.01–0.09	0.08–0.7	190–1500	PDMS
Kim [82]	Patterned wall	240	60	11.6	0.5	2784	PDMS
Sato [79]	Patterned wall	100	100	16.7	1.67	5500	PDMS–glass

[a]NA, not applicable.

structure [91] because a large difference in surface forces exists between the multiple immiscible phase flow. In [87], the prototype was made of PDMS and covered by a PMMA sheet. The approach utilized a hydrophobic microcapillary vent, which joins the two initial droplets. By introducing an effective dispersion coefficient inside a rectangular channel and simplifying the mass transport equation, Handique and Burns proposed an analytical model for droplet mixing actuated by thermocapillary [88]. Electrowetting can also be used to transport droplets [89]. Different mixing schemes can be used with this concept. Droplets can be merged and split repeatedly to generate the mixing pattern. For studying the mixing pattern inside the droplets, the reader is referred to [92]. The merged droplet can be transported around using electrowetting. Another approach for droplet mixing is to utilize the flow instability between two immiscible liquids [90, 91] or liquid–gas [93]. Through a carrier or sheath liquid such as oil, droplets of the aqueous samples were formed. While moving through the zigzag [90] or modified zigzag [94] shaped microchannel, the shear force difference between the wall and the sample accelerated the mixing process inside the droplet.

Table 7.5 Typical droplet micromixers.

Ref.	Transport type	Droplet size (nL)	Channel width (μm)	Channel height (μm)	Material
Hosokawa [87]	Pressure driven	10	100	150	PDMS/PMMA
Paik [89]	Electrowetting	1600	2480	600–1000	Glass
Song [90]	Multiple phases	75–150	20–100	NR[a]	PDMS

[a]NR, not reported.

Another effective strategy is to latinize gaseous slugs to create unsteady flow to enhance the mixing process [95]. The mixer had a serially connected O-shaped mixing channel. A focusing structure was used to form the bubble slugs. These slugs could split, stretch and fold the fluid inside the O-shaped mixing units and subsequently enhance the mixing process. Typical droplet micromixers are summarized in Table 7.5.

7.3 Active Micromixers

7.3.1 Pressure-induced Disturbance

Pressure-induced disturbance was one of the earliest investigated active micromixers. By modulating the pressure on the inlets of a T-mixer [96, 97] (Figure 7.9a), the mixing fluid was formed into serially segmented droplets along the mixing channel, which increased the contact surface significantly. The mixer was fabricated in silicon using DRIE and integrated in a microfluidic system. The pressure disturbance was produced by an integrated planar pump. This approach can also be realized through an external micropump [98]. Further, combining with focusing structure, Nguyen and Huang demonstrated a time-interleaved segmented micromixer [99] (Figure 7.9i). The mixing channel was fabricated on a polymer substrate and had a cross-section of 1 mm × 100 μm and was 50 mm long. The presssure disturbance was produced by two piezo discs glued on the mixer.

Another alterative approach to pressure disturbance is the introduction of pulsing velocity [100, 101] (Figure 7.9b). In [100], a simple T-mixer and simulation were shown with a pulsed side flow at a low *Re* of 0.3. Later, a computer-controlled source–sink system was used to generate pulsing velocity and further to obtain the pressure disturbance [101]. Details on this operation principle of a source–sink system can be found in [102]. The performance of the mixing process is dependent on the pulse frequency and the number of mixing units. In [103], the mixing pattern of this approach was extensively investigated using numerical simulation.

The pressure disturbance can also be introduced by directly moving the parts inside the mixing channel, which is similar to the commercial stirrer used on the macroscale. In [104], a micromixer was demonstrated using integrated conductors. A

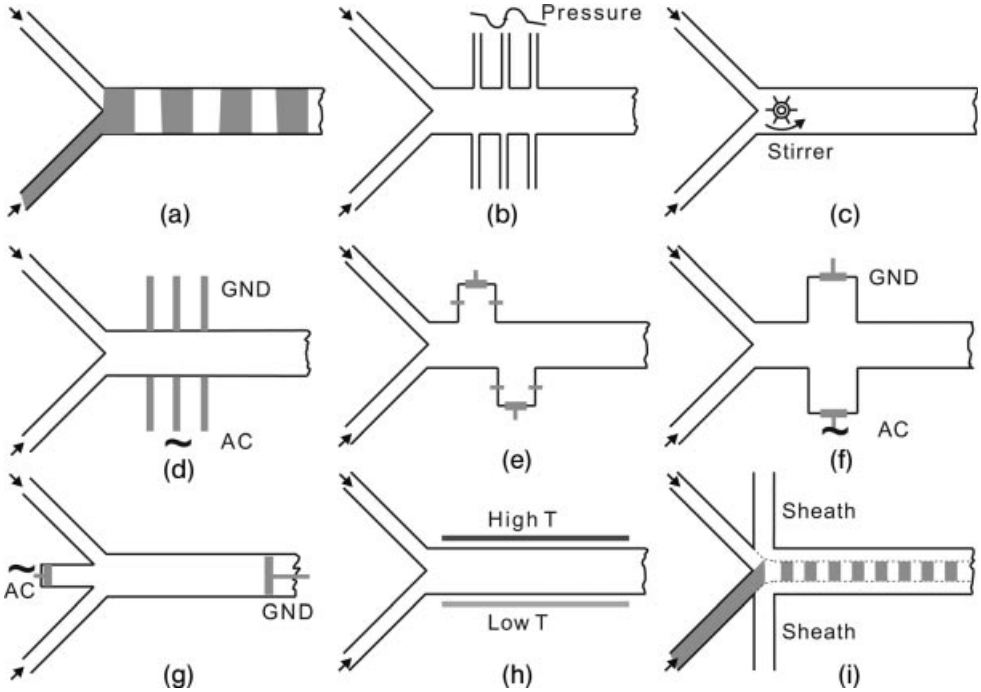

Figure 7.9 Active micromixers: (a) serial segmentation; (b) pressure disturbance along mixing channel; (c) integrated microstirrer in the mixing channel; (d) electrohydrodynamic disturbance; (e) dielectrophoretic disturbance; (f) electrokinetic disturbance in a mixing chamber; (g) electrokinetic disturbance in a mixing channel; (h) thermal disturbance; (i) combination of serial segmentation and focusing.

magnetic field was generated by these electrical conductors and moved magnetic beads 1–10 μm in diameter. The disturbance caused by the magnetic beads improved mixing significantly. Disturbance also was generated by an integrated micromachined magnetic microstirrer [105] (Figure 7.9c). The microstirrer was placed at the interface between two liquids in the mixing channel. An external magnetic field drove the stirrer at a speed between 100 and 600 rpm.

7.3.2 Electrohydrodynamic Disturbance

Similarly to the concept in [101], eletrohydrodynamic disturbance can be generated in the micromixer [106]. Instead of pressure sources, electrodes were placed along the mixing channel (Figure 7.9d). The mixing channel was 30 mm long, 250 μm wide and 250 μm deep. Numerous titanium wires were deposited in the direction perpendicular to the mixing channel. Good mixing could be obtained in less than 0.1s by adjusting the voltage and frequency on the electrodes at a low Re ($Re = 0.02$).

Dielectrophoresis (DEP) is a phenomenon in which a force is exerted on a dielectric particle when it is subjected to a non-uniform electric field. This effect causes the particle to move towards and against an electrode. Two prototypes based on DEP were reported in [107, 108]. With a combination of electrical actuation and local geometry channel variation, chaotic advection was generated by embedded particles for good mixing (Figure 7.9e).

In microfludics, electrokinetic flow, in addition to pressure-driven flow, is a major approach to transport tiny amounts of liquid in microchannels. Similarly to other pumping mechanisms, it can also be used to enhance the mixing process in micromixers. Jacobson *et al.* [41] reported electrokinectically driven mixing in a conventional T-mixer. Similarly to a pressure-driven T-mixer, throttle structures were still effective in the electrokinectically driven mixer [109]. In [110], the electrokinetic effect was used to disturb the pressure-driven flow in a micromixer. Another approach is to use oscillating electroosmotic flow in a mixing chamber via an AC voltage [111–113]. The pressure-driven flow becomes unstable in a mixing chamber (Figure 7.9f) or in a mixing channel (Figure 7.9g). Further details of this instability can be found in [114]. Similarly to the previous pressure-driven approach [96], switching on or off the voltage supplied to the flow generates fluid segments in the mixing channel [115, 116]. This flow modulation scheme was capable of injecting reproducible and stable fluid segments into microchannels. The working frequency in [115] was between 0.01 and 1 Hz and in [116] between 1 and 2 Hz. An approach involving modification of the zeta potential of the channel surface was also tried [117]. Of course, complex fabrication and a controlled mechanism were required for this approach. A simple but interesting approach is to utilize the oscillation inside the droplet using electrowetiing [118]. The introduced pattern can enhance mixing significantly.

7.3.3
Magnetohydrodynamic Disturbance

Magnetohydrodynamic-induced transversal and chaotic advection can be used in micromixers. With an external magnetic field, applied DC voltages on the electrodes generate Lorentz forces. The resulting Lorentz forces can roll and fold the liquids inside the mixing chamber and further enhance the mixing process [119, 120]. This concept only works with an electrolyte solution. The mixer in [119] was fabricated from co-fired ceramic tapes. The electrodes were printed with a gold paste. A fabrication process based on PDMS was also realized later [120]. Another approach is to introduce magnetic beads in the presence of a rotating magnetic field [121]. The mixer was achieved in a centrifugal platform made of PMMA.

7.3.4
Acoustic Disturbance

The proof of concept for acoustic mixing was reported by Moroney *et al.* [122] with a flexible-plate-wave (FPW) device. An analysis of the focused acoustic wave model in a

mixing chamber was proposed by Zhu and Kim [123]. They demonstrated an acoustic micromixer with a mixing chamber of 1 mm × 1 mm × 10 μm fabricated in silicon. The acoustic wave was generated by a zinc oxide membrane located at the bottom of the mixing chamber. The vibration could be adjusted by changing the frequency and voltage of the input signal. The concept of acoustic streaming was also used as an active mixing scheme [124]. Focused acoustic streaming could also be optimized by electrode patterns inside the mixing chamber [125]. In [126], glass and plastic substrates were tried to serve as a mixing chamber. However, due to energy absorption, the mixer fabricated on a plastic wafer had a lower performance that those fabricated on silicon or glass. In addition to the integrated design, stirring at high frequency can also be realized by an external pump [127].

It is noted that ultrasonic mixing may have some problems in applications in biological and chemical analysis. The first concern is the temperature rise caused by acoustic energy. Many biological fluids are highly sensitive to temperature. The second concern is ultrasonic waves around 50 kHz. These ultrasound waves may lead to cavitation, which is harmful to biological samples. To avoid these problems, Yasuda [128] used loosely focused acoustic waves to generate stirring movements. A piezoelectric zinc oxide thin film was used as an actuator, which was driven by a sinusoidal wave with frequencies corresponding to the thickness-mode resonance (e.g. 240 and 480 MHz) of the piezoelectric film. The results indicated that there was no significant temperature increase and the method could be used with temperature-sensitive fluids. Further acoustic microdevices for mixing water and ethanol and also water and uranine were reported [129, 130].

In addition to fluids, acoustic streaming induced around air bubbles could be used for mixing [131, 132]. In this mixer, cavities of 500 μm diameter and 500 μm depth were used to trap air bubbles. An integrated lead zirconate titanate (PZT) actuator was used in the design. Acoustic streaming was also used to disturb the flow in a conventional Y-mixer in [133]. Whereas the channel was made of PDMS, the acoustic actuator was integrated into the cover quartz wafer. An 8 μm thick zinc oxide layer with gold electrodes worked as the actuator. In [134], the use of a surface acoustic wave (SAW) approach was demonstrated for the mixing process. The SAW devices were fabricated on 128° Y-cut lithium niobate ($LiNbO_3$) and integrated in a PDMS-made prototype of microliter size. Another similar approach can be found in [135]. Typical active micromixers are summarized in Table 7.6.

7.3.5 Thermal Disturbance

Introducing thermal energy to form bubbles, a planar pulsed source–sink system was used to cause chaotic advection in a mixing chamber [136]. The mixer was fabricated in silicon on a 1 cm^2 area. The mixing chamber measured 1500 × 600 μm with a height of 100 μm. Another similar design [137] utilized a thermal bubble to generate disturbance in a mixing channel.

Since the diffusion coefficient and advection depend highly on temperature, the thermal field also can affect the mixing process strongly [138, 139]. Introducing a

Table 7.6 Typical active micromixers.

Ref.	Disturbance	Channel width (μm)	Channel height (μm)	Typical velocity (mm s^{-1})	Frequency (Hz)	*Re*	*Pe*	Material
Deshmukh [97]	Pressure	400	78	0.09	1	0.01	36	Silicon–glass
Fujii [98]	Pressure	150	150	0.9	100	0.13	133	PDMS
Glasgow [100]	Pressure	200	120	2	0.3	0.3	400	NA[a]
Okkels [103]	Pressure	200	26	1.6	0.85	0.04	321	PDMS
Suzuki [104]	Pressure	160	35	0.3	0.02	0.05	48	Silicon–glass
Lu [105]	Pressure	750	70	0.14	5	0.01	105	PDMS–glass
El Moctar [106]	EHD	250	250	4.2	0.5	0.02	1050	NA
Deval [107]	DEP	50	25	0.5	1	0.02	25	Si–SU8–glass
Lee [108]	EKD	200	25	0.5	1	0.01	100	NA
Oddy [111]	EKD	1000	300	0.5	10	0.15	1050	PDMS–glass
Tang [115]	EKD	500	35	1	0.17	0.04	509	PDMS–glass
Bau [119]	MHD	4700	1000	NR[a]	NR	NR	NR	Ceramic
Moroney [122]	Acoustic	1000	400	0.5	10	0.15	1050	Silicon–glass
Rife [124]	Acoustic	1600	1600	1	NR	1.6	1600	NR
Yasuda [128]	Acoustic	2000	2000	6.4	NR	12.8	12 800	Silicon–glass
Yang [130]	Acoustic	6000	60	0.5	NR	0.03	30	Silicon–glass
Liu [131]	Acoustic	15 000	300	5	NR	1.5	1500	Silicon–glass
Yaralioglu [133]	Acoustic	300	50	1	NR	0.86	300	PDMS–quartz
Evans [136]	Thermal	1500	100	NR	NR	NR	NR	Silicon–glass

[a]NR, not reported; NA, not applicable.

transverse temperature gradient [138] (Figure 7.9h), thermocapillary convection was investigated numerically. The analysis indicated that helical streamlines appeared inside the channel, which can increase the contact area between the mixing fluids inside. Using an infrared (IR) laser, an interfacial thermocapillary vortical flow was demonstrated for microfluidic mixing. The high gradient from the IR laser induced cavitation bubbles and further vortical flow, which in turn helped the mixing inside the fluid.

7.4 Fabrication Methods

Numerous fabrication techniques have been used for making micromixers. In the past few years, there have been two obvious developments in micromixer fabrication: the substrate was changed from silicon to polymers and the structures were changed from simple planar structure to complex 3D structure. Most of the early micromixers were fabricated in silicon. The mixing channels were either wet etched with KOH [16, 35, 42, 52, 53, 66] or dry etched using DRIE (deep reactive ion etching) [23, 26, 31, 37, 45, 54, 59, 96]. Anodically bonded glass on top of the channel

offered both sealing and optical access. Passive micromixers can be made entirely of glass [39–41]. Due to its electrically conducting properties, silicon cannot be used in applications with electrokinetic flows. Most active micromixers with integrated actuators were fabricated in silicon because the established technologies [104, 122, 127, 130], such as sputtering of metals and piezoelectric materials, are based on a silicon substrate.

However, silicon-based micromixers are relatively expensive because of the large surface area needed for microchannels and the required cleanroom facilities. Furthermore, silicon devices are chemically and biochemically not always compatible. Polymeric micromachining offers a lower fabrication cost and a faster prototyping cycle. A simple approach named soft lithography, established by Whitesides' group [140], has become very popular [25, 49, 74, 75, 111, 115]. In this approach, a lithography mask was printed using a high-resolution laser printer. Subsequently, the pattern was transferred to a negative expoxy photoresist of SU-8 on the silicon substrate. After developing and hard baking, the SU-8–silicon wafer worked as a master for subsequently elastomer replication. The elastomer most often used is polydimethylsiloxane (PDMS). PDMS can be sealed to glass reversibly by pressing the clean. PDMS and glass slides. This sealing can be used in some applications that do not involve high pressure. PDMS–glass or PDMS–PDMS can be sealed irreversibly via a surface treatment in an oxygen plasma. A high sealing strength can be achieved. PDMS is optically transparent to wavelengths above 280 nm. The mechanical rigidity of PDMS can adjusted by changing the ratio of the monomer and crosslinker. Normally, the more crosslinker is inside, the greater is the rigidity of PDMS. Further, several PDMS layers can be fabricated in the same way and bonded directly to form a complex three-dimensional structure [67, 70, 71, 82]. For PDMS–PDMS bonding, methanol could be used as a lubricant between the PDMS layers. Due to its sealing property, PDMS can also be used as the adhesion layer between glass and silicon [46] and some other materials.

Mixing channels were also fabricated by hot embossing with a hard template, which is micromachined in silicon [73] or nickel [63]. This approach can be adapted to injection molding for large-scale production. However, this approach is limited to a two-dimensional channel structure. Fast prototyping can be achieved with laser micromachining on thin polymer and adhesive sheets [19, 55]. This solution does not requires cleanroom facilities and expensive equipment. It is very suitable for academic research and earlier phototyping. However, the resolution of this approach is limited by the wavelength of the laser used).

7.5 Conclusion

The characteristic dimensionless numbers such as Reynolds number (*Re*) and Peclet number (*Pe*) are very suitable for discussing the operating conditions for micromixers. From the definitions in Equations (7.1) and (7.2), the relation

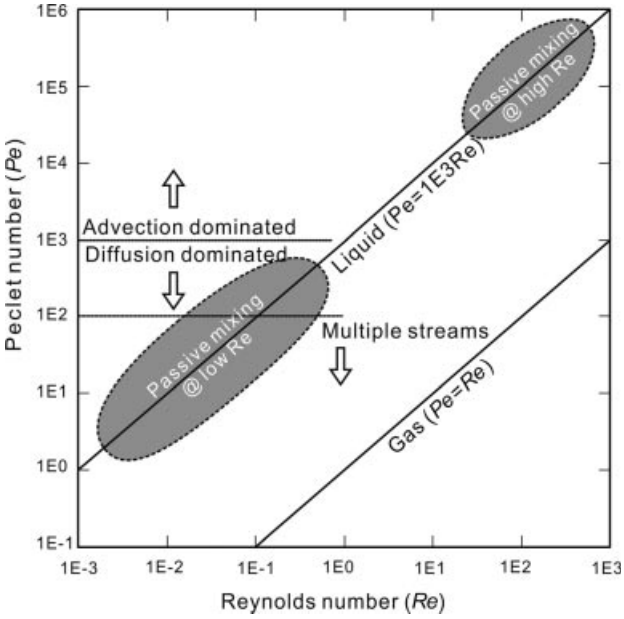

Figure 7.10 *Pe–Re* diagram.

between *Pe* and *Re* can be derived as

$$\frac{Pe}{Re} = \frac{L}{D_h}\frac{\nu}{D} \tag{7.12}$$

In micromixers, the hydraulic diameter D_h and the mixing path L are usually on the same order. Hence we can assume $L/D_h \approx 1$. For liquids, the kinematic viscosity is on the order $\nu = 10^{-6}\,m^2s^{-1}$ and the diffusion coefficient on the order $D = 10^{-9}\,m2s^{-1}$. Based on Equation (7.12), the relation between *Pe* and *Re* can be estimated as $Pe \approx 1000\,Re$ for liquids. On a *Pe–Re* diagram, the relation $Pe = 1000\,Re$ is represented by a straight line (Figure 7.10). The operating conditions of micromixers for liquids are expected to be around this line. Similarly, for gases with a typical kinematic viscosity and a diffusion coefficient of $\nu = 10^{-5}\,m^2\,s^{-1}$ and $D = 10^{-5}\,m^2\,s^{-1}$, respectively, the operating conditions can be expected to be around the line of $Pe = Re$.

List of Symbols and Abbreviations

Symbols

β	viscosity ratio of sheath flow to sample flow
η	dynamic viscosity (Pa s)

ν	kinematic viscosity ($m^2 s^{-1}$)
c	concentration of a species ($kg m^{-3}$)
c^*	dimensionless concentration
D	diffusion coefficient ($m^2 s^{-1}$)
D_h	hydraulic diameter (m)
H, h	channel height (m)
L	mixing path (m)
m	number of serial mixing stages
p	pressure (Pa)
Q	flow rate ($m^3 s^{-1}$)
r	mixing ratio
U	average flow velocity ($m s^{-1}$)
U	average flow velocity ($m s^{-1}$)
W	channel width (m)

Abbreviations

COC	cyclic olefin copolymer
DEP	dielectrophoresis
EHD	electrohydrodynamic disturbance
EKD	electrokinetic disturbance
FPW	flexible-plate-wave
IR	infrared
MEMS	microelectromechanical system
MHD	magnetohydrodynamic disturbance
PC	polycarbonate
PDMS	polydimethylsiloxane
Pe	Peclet number
PEO	poly(ethylene oxide)
PET	poly (ethylene terephthalate)
PETG	poly (ethylene terephthalate glycol)
PMMA	poly(methyl methacrylate)
PZT	lead zirconate titanate
Re	Reynolds number
SAW	surface acoustic wave
SEBS	polystyrene–(polyethylene/polybutylene)–polystyrene triblock copolymer

References

1 N. T. Nguyen, Z. G. Wu, Micromixers–a review, *J. Micromech. Microeng.*, **2005**, *15*, R1–R16.

2 M. J. Madou, *Fundamentals of Microfabrication: the Science of Miniaturization*, 2nd ed, CRC Press, Boca Raton, **2002**.

3 N. T. Nguyen, S. T. Wereley, *Fundamentals and Applications of Microfluidics*, 2nd edn, Artech House, Boston, **2006**.

4 M. Kakuta, F. G. Bessoth, A. Manz, Microfabricated devices for fluid mixing and their application for chemical synthesis. *Chem. Record*, **2001**, *1*, 395–405.

5 C. Erbacher, *et al.*, Towards Integrated Continuous-Flow Chemical Reactors. *Mikrochim. Acta*, **1999**, *131*, 19–24.

6 W. Ehrfeld, V. Hessel, H. Lowe, Microreactors: New Technology for Modern Chemistry, Wiley-VCH Verlag GmbH, Weiheim, **2000**.

7 A. J. deMello, Control and detection of chemical reactions in microfluidic systems. *Nature*, **2006**, *442*, 394–402.

8 A. Einstein, *Investigations on the Theory of the Brownian Movements*, Dover, New York, **1956**.

9 H. M. Ottino, Mixing, chaotic advection, and turbulence. *Annu. Rev. Fluid Mech.*, **1990**, *22*, 207–253.

10 R. S. Brodky, *Turbulence in Mixing Operations*, Academic Press, New York, **1975**.

11 J. M. Ottino, The mixing of fluids. *Sci. Am.*, January, **1989**, 55–67.

12 J. M. Ottino, *The Kinematics of Mixing: Stretching, Chaos, and Transport*, Cambridge University Press, New York, **1989**.

13 E. L. Cussler, *Diffusion Mass Transfer in Fluid Systems*, Cambridge University Press, New York, **1984**.

14 R. E. Cunningham, R. J. J. William, *Diffusion in Gases and Porous Media*, Plenum Press, New York. **1980**.

15 R. B. Bird, *et al.*, *Transport phenomena*, John Wiley & Sons, Inc., New York, **2002**.

16 A. E. Kamholz, *et al.*, Quantitative Analysis of molecular interactive in microfluidic channel: the T-sensor, *Anal. Chem.*, **1999**, *71*, 5340–5347.

17 A. E. Kamholz, P. Yager, Molecular diffusive scaling laws in pressure-driven microfluidic channels: deviation from one-dimensional Einstein approximations, *Sens. Actuators B*, **2002**, *82*, 117–121.

18 R. F. Ismagilov, *et al.*, Experimental and Theoretical Scaling Laws for Transverse Diffusive Broadening in Two-Phase Laminar Flows in Microchannels. *Appl. Phys. Lett.*, **2000**, *76*, 2376–2378.

19 Z. G. Wu, N. T. Nguyen, X. Y. Huang, Non-Linear Diffusive Mixing in Microchannels: Theory and Experiments. *J. Micromech. Microeng.*, **2004**, *14*, 604–611.

20 Z. G. Wu, N. T. Nguyen, Convective-diffusive transport in parallel lamination micromixers. *Microfluidics Nanofluidics*, **2005**, *1*, 208–217.

21 P. Hinsmann, *et al.*, Design, Simulation and Application of a New Micromixing Device for Time Resolved Infrared Spectroscopy of Chemical Reactions in Solutions. *Lab Chip*, **2001**, *1*, 16–21.

22 M. Yi, H. H. Bau, The Kinematics of Bend-Induced Mixing in Micro-Conduits. *Int. J. Heat Fluid Flow*, **2003**, *24*, 645–656.

23 S. H. Wong, M. C. L. Ward, C. W. Wharton, Micro T-Mixer as a Rapid Mixing Micromixer. *Sens. Actuators B*, **2004**, *100*, 365–385.

24 A. P. Sudarsan, V. M. Ugaz, Fluid mixing in planar spiral microchannels. *Lab Chip*, **2006**, *6*, 74–82.

25 D. S. W. Lim, *et al.*, Dynamic Formation of Ring-shaped Patterns of Colloidal Particles in Microfluidic Systems. *Appl. Phys. Lett.*, **2003**, *83*, 1145–1147.

26 S. Böhm, *et al.*, A Rapid Vortex Micromixer for Studying High-Speed Chemical Reactions, *MicroTAS2001*, Monterey, CA, **2001**, 25–27.

27 C.-H. Lin, C.-H. Tsai, L.-M. Fu, A rapid three-dimensional vortex micromixer ultilizing self-rotation effects under low Reynolds number conditions. *J. Micromech. Microeng.*, **2005**, *15*, 935–943.

28 S. H. Wong, *et al.*, Investigation of mixing in a cross-shaped micromixer with static mixing elements for reaction kinetics studies. *Sens. Actuators B*, **2003**, *95*, 414–424.

29 D. Gobby, P. Angeli, A. Gavriilidis, Mixing Characteristics of T-Type Microfluidic Mixers. *J. Micromech. Microeng.*, **2001**, *11*, 126–132.

30 I.-D. Yang, *et al.,* Surface tension driven and 3-D vortex enhanced rapid mixing microchamber. *J. Microelectromech. S.*, **2006**, *15*, 659–670.

31 T. T. Veenstra, Characterization Method for a New Diffusion Mixer Applicable in Micro Flow Injection Analysis Systems. *J. Micromech. Microeng.*, **1999**, *9*, 199–202.

32 N. Y. Lee, M. Yamada, M. Seki, Development of a passive micromixer based on repeated fluid twisting and flattening, and its application to DNA purification. *Anal. Bioanal. Chem.*, **2005**, *383*, 776–782.

33 R. J. Jackman, *et al.*, Microfluidic Systems with On-Line UV Detection Fabricated in Photodefineable Epoxy. *J. Micromech. Microeng.*, **2001**, *11*, 263–269.

34 H. Möbius, *et al.,* Sensor Controlled Processes in Chemical Microreactors, in *Proceedings of Transducers '95 Stockholm*, **1995**, 775–778.

35 M. Koch, *et al.,* Improved Characterization Technique for Micromixers. *J. Micromech. Microeng.*, **1999**, *9*, 156–158.

36 V. Haverkamp, *et al.,* The Potential of Micromixers for Contacting of Disperse Liquid Phases, *Fresenius J. Anal. Chem.*, **1999**, *364*, 617–624.

37 F. G. Bessoth, A. J. deMello, A. Manz, Microstructure for Efficient Continuous Flow Mixing. *Anal. Commun.*, **1999**, *36*, 213–215.

38 M. Kakuta, *et al.,* Micromixer-Based Time-Resolved NMR: Applications to Ubiquitin Protein Conformation. *Anal. Chem.*, **2003**, *75*, 956–960.

39 K. Fluri, *et al.,* Integrated Capillary Electrophoresis Devices with an Efficient Postcolumn Reactor in Planar Quartz and Glass Chips. *Anal. Chem.*, **1996**, *68*, 4285–4290.

40 A. G. Hadd, *et al.,* Microchip Device for Performing Enzyme Assays. *Anal. Chem.*, **1997**, *69*, 3407–3412.

41 S. C. Jacobson, T. E. McKnight, J. M. Ramsey, Microfluidic Devices for Electrokinematically Driven Parallel and Serial Mixing. *Anal. Chem.*, **1999**, *71*, 4455–4459.

42 R. Miyake, *et al.,* Micro Mixer with Fast Diffusion, in *Proceedings of MEMS'93*, San Diego, CA, **1993**, 248–253.

43 U. D. Larsen, W. Rong, P. Telleman, Design of Rapid Micromixers Using CFD, in *Proceedings of Transducers '99 Sendai*, **1999**, 200–203.

44 R. U. Seidel, *et al.,* Capilary Force Mixing Device as Sampling Module for Chemical Analysis, in *Proceedings of Transducers '99 Sendai*, **1999**, 438–441.

45 J. Voldman, M. L. Gray, M. A. Schmidt, An Integrated Liquid Mixer/Valve. *J. Microelectromech. Syst.*, **2000**, *9*, 295–302.

46 J. B. Knight, A. Vishwanath, J. P. Brody, R. H. Austin, Hydrodynamic Focusing on a Silicon Chip: Mixing Nanoliters in Microseconds. *Phys. Rev. Lett.*, **1998**, *80*, 3863–3866.

47 Z. G. Wu, N. T. Nguyen, Hydrodynamic focusing in microchannels under consideration of diffusive dispersion: theories and experiments. *Sens. Actuators B*, **2005**, *107*, 965–974.

48 K. Jensen, Chemical kinetics: Smaller, faster chemistry. *Nature*, **1998**, *393*, 735–736.

49 G. M. Walker, D. J. Ozers, D. J. Beebe, Cell Infection Within a Microfluidic Device Using Virus Gradients. *Sens. Actuators B*, **2004**, *98*, 347–355.

50 Z. G. Wu, N. T. Nguyen, Rapid mixing using two-phase hyraulic focusing in microchannels. *Biomed. Microdev.*, **2005**, *7*, 13–20.

51 H. Y. Park, *et al.,* Achieving uniform mixing in a microfluidic devices: hydrodynamic focusing prior ro mixing. *Anal. Chem.*, **2006**, *78*, 4465–4473.

52 J. Branebjerg, *et al.,* Fast Mixing by Lamination, in *Proceedings of MEMS'96, San Diego, CA*, **1996**, 441–446.

53 N. Schwesinger, *et al.,* A Modular Microfluid System with an Integrated Micromixer. *J. Micromech. Microeng.*, **1996**, *6*, 99–102.

54 B. L. Gray, *et al.,* Novel Interconnection Technologies for Integrated Microfluidic Systems. *Sens. Actuators A*, **1999**, *77*, 57–65.

55 M. S. Munson, P. Yager, Simple Quantitative Optical Method for Monitoring the Extent of Mixing Applied to a Novel Microfluidic Mixer. *Anal. Chim. Acta*, **2004**, *507*, 63–71.

56 B. He, *et al.,* A Picoliter-Volume Mixer for Microfluidic Analytical Systems. *Anal. Chem.*, **2001**, *73*, 1942–1947.

57 J. Melin, *et al.,* A Fast Passive and Planar Liquid Sample Micromixer. *Lab Chip*, **2004**, *4*, 214–218.

58 H. Wang, *et al.,* Optimizing Layout of Obstacles for Enhanced Mixing in Microchannels. *Smart Mater. Struct.*, **2002**, *11*, 662–667.

59 Y. Lin, *et al.,* Ultrafast Microfluidic Mixer and Freeze-Quenching Device. *Anal. Chem.*, **2003**, *75*, 5381–5386.

60 V. Mengeaud, J. Josserand, H. H. Girault, Mixing Processes in a Zigzag Microchannel: Finite Element Simulation and Optical Study. *Anal. Chem.*, **2002**, *74*, 4279–4286.

61 S. Jeon, *et al.,* Optically fabricated three dimensional nanofluidic mixers for microfluidic devices. *Nano Lett.*, **2005**, *5*, 1351–1356.

62 S. W. Jones, O. M. Thomas, H. Aref, Chaotic Advection by Laminar Flow in a Twisted Pipe. *J. Fluid Mech.*, **1989**, *209*, 335–357.

63 C. C. Hong, J. W. Choi, C. H. Ahn, A novel in-plane microfluidic mixer with modified tesla structure. *Lab Chip*, **2004**, *4*, 109–113.

64 M. K. Jeon, *et al.,* Design and characterization of a passive recyle micromixer. *J. Micromech. Microeng.*, **2005**, *15*, 346–350.

65 U. Gebhard, H. Hein, U. Schmidt, Numerical investigation of fluidic micro-osillators. *J. Micromech. Microeng.*, **1996**, *6*, 115–117.

66 R. H. Liu, Passive Mixing in a Three-Dimensional Serpentine Microchannel. *J. Microelectromech. Syst.*, **2000**, *9*, 190–197.

67 R. A. Vijiayendran, *et al.,* Evaluation of a Three-Dimensional Micromixer in a Surface-Based Biosensor. *Langmuir*, **2003**, *19*, 1824–1828.

68 D. S. Kim, S. H. Lee, T. H. Kwon, C. H. Ahn, A serpentine laminating micromixer combining splitting/recombination and advection. *Lab Chip*, **2005**, *5*, 739–747.

69 D. J. Kim, *et al.,* An easily integrative and efficient micromixer and its application to the spectroscopic detection of glucose-catalyst reactions. *Analyst*, **2005**, *130*, 293–298.

70 H. Chen, J. C. Meiners, Topologic Mixing on a Microfluidic Chip. *Appl. Phys. Lett.*, **2004**, *84*, 2193–2195.

71 S. J. Park, *et al.,* Rapid Three-Dimensional Passive Rotation Micromixer Using the Brackup Process. *J. Micromech. Microeng.*, **2004**, *14*, 6–14.

72 C. P. Jen, *et al.,* Design and Simulation of the Micromixer with Chaotic Advection in Twisted Microchannels. *Lab Chip*, **2003**, *3*, 77–81.

73 T. J. Johnson, D. Ross, L. E. Locascio, Rapid Microfluidic Mixing. *Anal. Chem.*, **2002**, *74*, 45–51.

74 A. D. Stroock, *et al.,* Chaotic Mixer for Microchannels. *Science*, **2002**, *295*, 647–451.

75 A. D. Stroock, G. M. Whitesides, Controlling Flows in Microchannels with Parterned Surface Charge and Topography. *Acc. Chem. Res.*, **2003**, *36*, 597–604.

76 P. B. Howell, Jr. *et al.,* A microfluidic mixer with grooves placed on the top and bottom of the channel. *Lab Chip*, **2005**, *5*, 524–530.

77 H. Wang, *et al.,* Numerical Investigation of Mixing in Microchannels with Patterned Grooves. *J. Micromech. Microeng.*, **2003**, *13*, 801–808.

78 D. Lim, *et al.,* Fabrication of Microfluidic Mixers and Artificial Vasculatures Using a High-Brightness Diode-Pumped Nd:YAG

Laser Direct Write Method. *Lab Chip*, **2003**, *3*, 318–323.

79 H. Sato, *et al.*, Improved inclined multi-lithography using water as exposure medium and its 3D mixing microchannel application. *Sens. Actuators A*, **2006**, *128*, 183–190.

80 E. Biddiss, D. Erickson, D. Li, Heterogeneous Surface Charge Enhanced Micromixing for Electrokinetic Flows. *Anal. Chem.*, **2004**, *76*, 3208–3213.

81 W. I. Hau, *et al.*, Surface-Chemistry Technology for Microfluidics. *J. Micromech. Microeng.*, **2003**, *13*, 272–278.

82 D. S. Kim, *et al.*, A Barrier Embedded Chaotic Micromixer. *J. Micromech. Microeng.*, **2004**, *14*, 798–805.

83 A. Bertsch, *et al.*, Static Micromixers Based on large-Scale Industrial Mixer Geometry. *Lab Chip*, **2001**, *1*, 56–60.

84 A. Bertsch, *et al.*, Laminar flow in static mixer with helical elements, **1998**, http://www.bakker.org/cfmbook/lamstat.pdf.

85 T. Cubaud, T. G. Mason, Folding of viscous threads in diverging microchannels. *Phys. Rev. Lett.*, **2006**, *96*, 114501.

86 H. Y. Gan, Y. C. Lam, N. T. Nguyen, Polymer-based device for efficient mixing of viscoelastic fluids. *Appl. Phys. Lett.*, **2006**, *88*, 224103.

87 K. Hosokawa, T. Fujii, I. Endo, Droplet-based nano/picoliter mixer using hydrophobic microcapillary vent, in *Proceedings of MEMS'96*, **1999**, *Piscataway, NJ*, 388–393.

88 K. Handique, M. A. Burns, Mathematical Modeling of Drop Mixing in a Slit-Type Microchannel. *J. Micromech. Microeng.*, **2001**, *11*, 548–554.

89 P. Paik, V. K. Pamula, R. B. Fair, Rapid Droplet Mixers for Digital Microfluidic Systems. *Lab Chip*, **2003**, 253–259.

90 H. Song, *et al.*, Experimental Test of Scaling of Mixing by Chaotic Advection in Droplets Moving Through Microfluidic Channels. *Appl. Phys. Lett.*, **2003**, *83*, 4664–4666.

91 J. D. Tice, A. D. Lyon, R. F. Ismagilov, Effects of Viscosity on Droplet Formation and Mixing in Microfluidic Channels. *Anal. Chim. Acta*, **2003**, *507*, 73–77.

92 Z. B. Stone, H. A. Stone, Imaging and quantifying mixing in a model droplet micromixer. *Phys. Fluids*, **2005**, *17*, 063103.

93 A. Gunther, *et al.*, Micromixing of miscible liquids in segmented gas–liquid flow. *Langmuir*, **2005**, *21*, 1547–1555.

94 A. Liau, *et al.*, Mixing crowded biological solution in milliseconds. *Anal. Chem.*, **2005**, *77*, 7618–7625.

95 P. Garstecki, M. A. Fischbach, G. M. Whitesides, Design for mixing using bubbles in branched microfluidic channels. *Appl. Phys. Lett.*, **2005**, *86*, 244108.

96 A. A. Deshmukh, D. Liepmann, A. P. Pisano, Continuous Micromixer with Pulsatile Micropumps in *Technical Digest of the IEEE Solid State Sensor and Actuator Workshop*, Hilton Head Island, SC, **2000**, 73–76.

97 A. A. Deshmukh, D. Liepmann, A. P. Pisano, Characterization of a Micro-Mixing, Pumping, and Valving System, in *Proceedings of Transducers '01, Munich*, **2001**, 779–782.

98 T. Fujii, *et al.*, A Plug and Play Microfluidic Device. *Lab Chip*, **2003**, *3*, 193–197.

99 N. T. Nguyen, X. Huang, Mixing in microchannels based on hydrodynamic focusing and time-interleaved segmentation: modelling and experiment. *Lab Chip*, **2005**, *5*, 1320–1326.

100 I. Glasgow, N. Aubry, Enhancement of Microfluidic Mixing Using Time Pulsing. *Lab Chip*, **2003**, *3*, 114–120.

101 X. Z. Niu, Y. K. Lee, Efficient Spatial-Temporal Chaotic Mixing in Microchannels. *J. Micromech. Microeng.*, **2003**, *13*, 454–462.

102 S. Johnes, H. Aref, Chaotic Advection in Pulsed Source-Sink Systems. *Phys. Fluids*, **1988**, *31*, 469–485.

103 F. Okkels, P. Tabeling, Spatiotemporal Resonances in Mixing of Open

Viscous Fluidis. *Phys. Rev. Lett.*, **2004**, *92*, 038301.

104 H. Suzuki, C. M. Ho, A Magnetic Force Driven Chaotic Micro-Mixer, in *Proceedings of MEMS'02, Las Vegas*, **2002**, 40–43.

105 L. H. Lu, K. S. Ryu, C. Liu, A Magnetic Microstirrer and Array for Microfluidic Mixing. *J. Microelectromech. S.*, **2002**, *11*, 462–469.

106 A. O. El Moctar, N. Aubry, J. Batton, Electro-Hydrodynamic Micro-fluidic Mixer. *Lab Chip*, **2003**, *3*, 273–280.

107 J. Deval, P. Tabeling, C. M. Ho, A Dielectrophoretic Chaotic Mixer, in *Proceedings of MEMS'02* Las Vegas **2002**, 36–39.

108 Y. K. Lee, *et al.,* Chaotic Mixing in Electrokinetically and Pressure Driven Micro Flows, in *Proceedings of MEMS'01, Interlaken*, **2001**, 483–486.

109 M. Z. Huang, *et al.,* Application of elctrokinetic instability flow for enhanced micromixing in cross-shaped microchannel. *Biomed. Microdev.*, **2006**, *8*, 309–315.

110 G. L. Letteri, *et al.,* Consequences of opposing electrokinetically and pressure-induced flows in microchannels of varying geometries in *Proceedings of MicroTAS2000, Enschede*, **2000**, 351–354.

111 M. H. Oddy, J. G. Santiago, J. C. Mikkelsen, Electrokinetic Instability Micromixing. *Anal. Chem.*, **2001**, *73*, 5822–5832.

112 L.-M. Fu, *et al.,* A novel microfluidic mixer utilizing electrokinetic driving forces under low switching frequency. *Electrophoresis*, **2005**, *26*, 1814–1824.

113 X. Z. Niu, *et al.,* Active microfluidic mixer chip. *Appl. Phys. Lett.*, **2006**, *88*, 153508.

114 C. H. Chen, *et al.,* Convective and absolute electrokinetic instability with conductivity gradients. *J. Fluid Mech.*, **2005**, *524*, 263–303.

115 Z. Tang, *et al.,* Electrokinetic Flow Control for Composition Modulation in a Microchannel. *J. Micromech. Microeng.*, **2002**, *12*, 870–877.

116 J. T. Coleman, J. mcKechnie and D. Sinton, High-efficienciency electrokinetic micromixing through symmetric sequenctial jnjection and expansion. *Lab Chip*, **2006**, *6*, 1033–1039.

117 J.-L. Lin. K. H. Lee, G.-B. Lee, Active mixing inside microchannels utilizing dynamic variation of gradient zeta potentials. *Electrophoresis*, **2005**, *26*, 4605–4615.

118 F. Mugele, J.-C. Baret, D. Steinhauser, Microfluidic mixing through electrowetting-induced droplet oscillations. *Appl. Phys. Lett.*, **2006**, *88*, 204106.

119 H. H. Bau, J. Zhong, M. Yi, A Minute Magneto Hydro Dynamic (MHD) Mixer. *Sens. Actuators B*, **2001**, *79*, 207–215.

120 S. Qian, H. H. Bau, Magneto-Hydrodynamic stirrer for stationary and moving fluids. *Sens. Actuators B*, **2005**, *106*, 859–870.

121 M. Grumann, *et al.,* Batch-mode mixing on centrifugal microfluidic platforms. *Lab Chip*, **2005**, *5*, 560–565.

122 R. M. Moroney, R. M. White, R. T. Howe, Ultrasonically Induced Microtransport, in *Proceedings of MEMS'91, Nara*, **1991**, 277–282.

123 X. Zhu, E. S. Kim, Acoustic-wave liquid mixer, in *Microelectromechanical Systems (MEMS)*, American Society of Mechanical Engineers, Dynamic Systems and Control Division (Publication) DSC v 62. ASME, Fairfield. NJ, **1997**, 35–38.

124 J. C. Rife, *et al.,* Miniature Valveless Ultrasonic Pumps and Mixers Sens., *Actuators A*, **2000**, *86*, 135–140.

125 V. Vivek, Y. Zeng, E. S. Kim, Novel Acoustic-Wave Micromixer, in *Proceedings of MEMS'00 Miyazaoi*, **2000**, 668–673.

126 H. Yu, J. W. Kwon, E. S. Kim, Microfluidic mixer and transporter based on PZT self-focusing acoustic transducers. *J. Microelectromech. Syst.*, **2006**, *15*, 1015–1024.

127 P. Woias, K. Hauser, F. Yacoub-George, An Active Silicon Micromixer for mTAS

Applications, MicroTAS 2000, (Boston MA), **2000**, 277–282.

128 K. Yasuda, Non-Destructive, Non-Contact Handling Method for Biomaterials in Micro-Chamber by Ultrasound. *Sens. Actuators B*, **2000**, *64*, 128–135.

129 Z. Yang, *et al.*, Active Micromixer for Microfluidic Systems Using Lead-Zirconate-Ttitanate (PZT)-Generated Ultrasonic Vibration. *Electrophoresis*, **2000**, *21*, 116–119.

130 Z. Yang, *et al.*, Ultrasonic Micromixer for Microfluidic Systems. *Sens. Actuators A*, **2001**, *93*, 266–272.

131 R. H. Liu, *et al.*, Bubble-Induced Acoustic Micromixing. *Lab Chip*, **2002**, *2*, 151–157.

132 R. H. Liu, *et al.*, Hybridization Enhancement Using Cavitation Microstreaming. *Anal. Chem.*, **2003**, *75*, 1911–1917.

133 G. G. Yaralioglu, *et al.*, Ultrasonic Mixing in Microfluidic Channels Using Integrated Transducers. *Anal. Chem.*, **2004**, *76*, 3694–3698.

134 W.-K. Tseng, *et al.*, Active micro-mixers using surface acoustic waves on Y-cut 128° $LiNbO_3$. *J. Micromech. Microeng.*, **2006**, *16*, 539–548.

135 K. Sritharan, *et al.*, Active mixing at low Reynold's numbers. *Appl. Phys. Lett.*, **2006**, *88*, 054102.

136 J. Evans, D. Liepmann, A. P. Pisano, Planar Laminar Mixer, in *Proceedings of ME1MS'97, Nagoya*, **1997**, 96–101.

137 J. H. Tsai, L. Lin, Active microfluidic mixer and gas bubble filter drivern by thermal bubble pump. *Sens. Actuators A*, **2002**, *97–98*, 665–671.

138 A. A. Darhuber, Microfluidic actuation by modulation of surface stresses. *Appl. Phys. Lett.*, **2003**, *82*, 657–659.

139 R. Muruganathan, Y. Zhang, T. M. Fischer, Interfacial thermocapillary vortical flow for microfluidic mixing. *J. Am. Chem. Soc.*, **2006**, *128*, 3474–3475.

140 D. Duffy, J. McDonald, O. Schueller, G. M. Whitesides, Rapid prototyping of microfluidic systems in poly(dimethylsiloxane). *Anal. Chem.*, **1998**, *70*, 4974–4984.